Opto-Electronic Engineering

Article

2017, Vol 44, Issue 3

Symmetry breaking of photonic spin-orbit interactions in metasurfaces

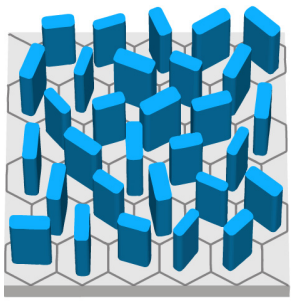

Fei Zhang[1,2], Mingbo Pu[1], Jun Luo[1], Honglin Yu[2] and Xiangang Luo[1]*

[1] State Key Laboratory of Optical Technologies on Nano-Fabrication and Micro-Engineering, Institute of Optics and Electronics, Chinese Academy of Sciences, Chengdu 610209, China; [2]Key Laboratory of Optoelectronic Technology and System, Ministry of Education, Chongqing University, Chongqing 400044, China

Abstract: Spin-orbit optical phenomena pertain to the wider class of electromagnetic effects originating from the interaction of the photon spin with the spatial structure and propagation characteristics of an optical wave, mediated by suitable optical media. There are many emerging photonic applications of spin-orbit interactions (SOI) of light, such as control of the optical wave propagation via the spin, enhanced optical manipulation, and generation of structured optical fields. Unfortunately, current applications are based on symmetric SOI, that is, the behaviours of polarized photons with two opposite spins are opposite, leading to the limit of spin-based multiplexers. The symmetry of SOI can be broken in our proposed metasurfaces, consisting of spatially varying birefringence, which can arbitrarily and independently build SOI for two opposite spins without reduction of optical energy usage. We obtain three kinds of dual-functional metasurfaces at visible and infrared wavelengths with high efficiency. Our concept of generation of asymmetric SOI for two spins, using anisotropic metasurfaces, will open new degrees of freedoms for building new types of spin-controlled multifunctional shared-aperture devices for the generation of complex structured optical fields.

Keywords: metasurfaces; metamaterials; spin-orbit interactions

DOI: 10.3969/j.issn.1003-501X.2017.03.006 **Citation:** *Opto-Elec Eng*, 2017, **44**(3): 319−325

1 Introduction

The optical spin-orbit interactions (SOI), describing the coupling between the spin and orbit degrees of freedom of photons during the transport of light, was first introduced in 1992 by Liberman and Zel'dovich [1]. Light can transport angular momentum through two different components, namely spin angular momentum (SAM) and orbital angular momentum (OAM) [2]. SAM can be $\sigma = \pm 1$ per photon (hereafter we consider dynamical quantities per photon in units of $\hbar = 1$), depending on the handedness of the circular polarization, while OAM has an unbounded value of l per photon [3], where l (an integer) is known as topological charge of the light. The interplay and mutual conversion between SAM and OAM represent SOI of light, and geometric phase, originating from the coupling between SAM and coordinate frame rotation, underlies the spin-dependent deformations of optical field.

Metasurfaces [4-5] are composed of a dense arrangement of resonant antennas on a sub-wavelength scale, which have huge fascinations and prospects to achieve miniaturization and integration. Recently, metasurfaces have been utilized to realize flat lenses [6-9], vortex generators [10-14], polarization controllers [15-16], optical holograms [17-19], virtual shaping [20] and electromagnetic illusion [21]. Most importantly, metasurfaces, consisting of properly designed anisotropic sub-wavelength antennas, allow considerable enhancement of the SOI effects. Such metasurfaces transform incident circularly polarized (CP) light into transmitted light with opposite helicity, imprinted with a geometric phase $2\sigma\theta$ [22-23], where θ is the orientation of antenna. Thus, varying the orientation of anisotropic antenna is an efficient approach for achieving spin-dependent shaping of light. However, it also results in symmetrical SOI of light for two opposite spins, such as the anisotropy-induced spin Hall effect [24-27]. The right and left circularly polarized (RCP and LCP) beams are

Received 24 November 2016; accepted 15 January 2017
* E-mail: lxg@ioe.ac.cn

deflected in opposite directions. Additionally, the optical vortex beams generated from the conventional metasurfaces mentioned above are always in pairs with opposite topological charges [11-12], and the holographic images for two opposite spins are central symmetric [17-18]. In a word, the symmetry of SOI for two opposite spins may pose obstacles for multi-function integration. For example, traditional methods of achieving spin-selective focusing and imaging, based on anisotropic structured metasurfaces, are combining the two sets of patterns in a shared aperture without overlapping each other. Thus, the transmitted light consists of not only the focused but also the scattered light because of the inversion symmetry of phase gradient, leading to low optical efficiency and high background noise.

In fact, metasurfaces have high degree of freedom to control the wavefront of electromagnetic waves. The local phase pickup can be manipulated not only through the geometric phase concept but also by tailoring other properties, such as material, shape and size. The latter one can produce an additional spin-independent phase gradient in the transmitted or reflected light [12, 14]. In this paper, the spin-independent phase gradient as well as the geometric phase is merged in our proposed all-dielectric metasurfaces. Therefore, the total phase gradient is also spin-dependent but independent for two converted spins, that is, our proposed metasurfaces have the capabilities of producing arbitrary combination of wavefronts for these two converted spins, resulting in asymmetric SOI of light. As a proof-of-concept, we apply our proposed design principle to theoretically achieve asymmetric holographic images, spin-selective focusing without the scattered noise, and generation of vortex beams with asymmetric topological charges at visible and infrared wavelengths (λ = 532 nm and 10.6 μm) with high efficiency, showing that our concept may provide new opportunities to realize asymmetric SOI for various practical applications of interest. Our proposed design may open a new degree of freedom for the photonic applications of SOI and the design of multifunctional shared-aperture metasurfaces.

2 Theoretical analyses

To present the operation of the SOI in anisotropic structured metasurfaces, we begin with analysis of a single anisotropic optical scatterer. For simplicity, we assume a transparent anisotropic scatterer that can introduce phase shifts $\phi\pm\delta/2$ for two orthogonal polarizations along the major and minor axes, respectively. Thus, the Jones matrix can be described as diag[(exp(iϕ+iδ/2), exp(iϕ–iδ/2)]. Then, performing a rotation by the angle θ with respect to x-direction and also working with the helicity basis, in which $|L\rangle=(0\ 1)^{\mathrm{T}}$ and $|R\rangle=(1\ 0)^{\mathrm{T}}$ denote LCP and RCP components, respectively. The transmission matrix $\boldsymbol{T}$ using the Jones calculus has the explicit form [11]:

$$\boldsymbol{T}=\exp(\mathrm{i}\phi)\begin{bmatrix}\cos\dfrac{\delta}{2} & \mathrm{i}\sin\dfrac{\delta}{2}\exp(\mathrm{i}2\theta)\\ \mathrm{i}\sin\dfrac{\delta}{2}\exp(-\mathrm{i}2\theta) & \cos\dfrac{\delta}{2}\end{bmatrix}. \quad (1)$$

Thus, if a beam with arbitrary polarization $\boldsymbol{E}_{\mathrm{i}}$ is normally incident on metasurface, the resulting beam $\boldsymbol{E}_{\mathrm{o}}$ can be written as:

$$\begin{aligned}\boldsymbol{E}_{\mathrm{o}}=\boldsymbol{T}\boldsymbol{E}_{\mathrm{i}}=\cos\frac{\delta}{2}\exp(\mathrm{i}\phi)\boldsymbol{E}_{\mathrm{i}}-\mathrm{i}\sin\frac{\delta}{2}\times\\ [\langle\boldsymbol{E}_{\mathrm{i}}\,|\,R\rangle\exp(-\mathrm{i}2\theta+\mathrm{i}\phi)\,|\,L\rangle+\\ \langle\boldsymbol{E}_{\mathrm{i}}\,|\,L\rangle\exp(\mathrm{i}2\theta+\mathrm{i}\phi)\,|\,R\rangle]\ .\end{aligned} \quad (2)$$

The first term indicates the scattered beams with the same spin as the incidence, and the second term represents the scattered beams with the opposite spin. Here, the phase factors exp(±i2θ), originating from geometric phases, depend on the rotation of the scatterer, appearing in the transmitted light with opposite helicity. In the past studies of SOI in anisotropic structured metasurfaces, the phase factor exp(iϕ) is ignored, because it is considered as constant for one properly designed scatterer even with a varying orientation. As a result, each anisotropic scatterer with a certain rotation angle operates as a local circular birefringence with opposite phase shifts for two opposite spins, resulting in inversely symmetric phase gradient for an array of the scatterers, which is the main reason of the symmetry of SOI for two opposite spins. Obviously, the symmetry breaking of SOI can be developed by the absence of inversion symmetry of phase gradient, which can be achieved by introducing a tunable spin-independent phase ϕ via tailoring the scatterer's size [12, 14]. In this case, the total phase gradient for the cross-polarized elements of transmitted light should be described as $2\sigma\theta+\phi$.

Fig. 1(a) shows a schematic diagram of our proposed all-dielectric metasurface platform. The building blocks of the metasurface are an array of high-aspect-ratio dielectric chamfered nanofins on a substrate, with same height H and chamfering radius R, but different geometries (width W and length L) and orientations θ (Figs. 1(c)~1(e)). The nanofins are placed at the center of hexagonal unit cells with a lattice constant P (Figs. 1(a) and 1(b)). The total phase gradient is composed of spin-dependent geometric phase and spin-independent phase imparted via rotation of nanofin and tailoring of size, respectively. Meanwhile, in order to maximize cross-polarized transmissivity, the nanofins should act as half-waveplates by tailoring the aspect ratio (L/ W).

We carefully designed eight unit cells at the wavelengths of 532 nm and 10.6 μm, with an incremental spin-independent phase of ~π/4 between adjacent nanofins. Figs. 1(f) and 1(g) show the simulated results at the wavelengths of 532 nm and 10.6 μm, respectively. The conversion efficiencies are quite high (average conversion efficiencies are ~94.2% and ~92.7% for λ= 532 nm and λ= 10.6 μm, respectively), and each unit cell almost

works as local half-wave plate. It is obvious that both spin-dependent geometric phase and spin-independent phase can cover the entire 0~2π range by rotating each nanofin from −π/2 to π/2 and proper geometries of unit cell mentioned above. Furthermore, such nanofins operate as weakly coupled low-quality-factor Fabry-Pérot resonators [28], so both spin-independent phases and cross-polarized transmissivities almost do not vary with rotation angle θ, which provides convenience for obtainment of any combination of spin-independent phase gradient and spin-dependent phase gradient.

Here, considering that all the nanofins simultaneously contribute to the desired wavefront of the two CP incidences, the selection of nanofin and its orientation at coordinate (x, y) can be written as

$$\phi = \frac{1}{2}[(\psi_1 - 2n_1\pi) + (\psi_{-1} - 2n_{-1}\pi)] \quad , \tag{3}$$

$$\theta = \frac{1}{4}[(\psi_{-1} - 2n_{-1}\pi) - (\psi_1 - 2n_1\pi)] \quad , \tag{4}$$

where $\psi_1(x, y)$ and $\psi_{-1}(x, y)$ are, respectively, desired independent phase distributions for $\sigma = \pm 1$; n_1 and n_{-1} are two integers. The obtained spin-independent phases are then quantized into eight values, ranging from 0 to 2π, and the eight unit cells mentioned earlier, with proper orientations θ, are used to fill the corresponding positions, leading to desired SOI of light for two opposite spins.

3 Results and discussion

The freedom provided by the proposed platform for independent manipulation of spin-dependent and spin-independent phases allows a wide variety of asymmetric SOI for two opposite spins. To demonstrate the versatility and high performance of this platform, we numerically achieve three kinds of spin-controlled dual-functional devices for visible and infrared wavelengths, which can lead to asymmetric holographic images, spin-selective focusing without the scattered noise, and generation of vortex beams with asymmetric topological charges, respectively. All the calculations are based on

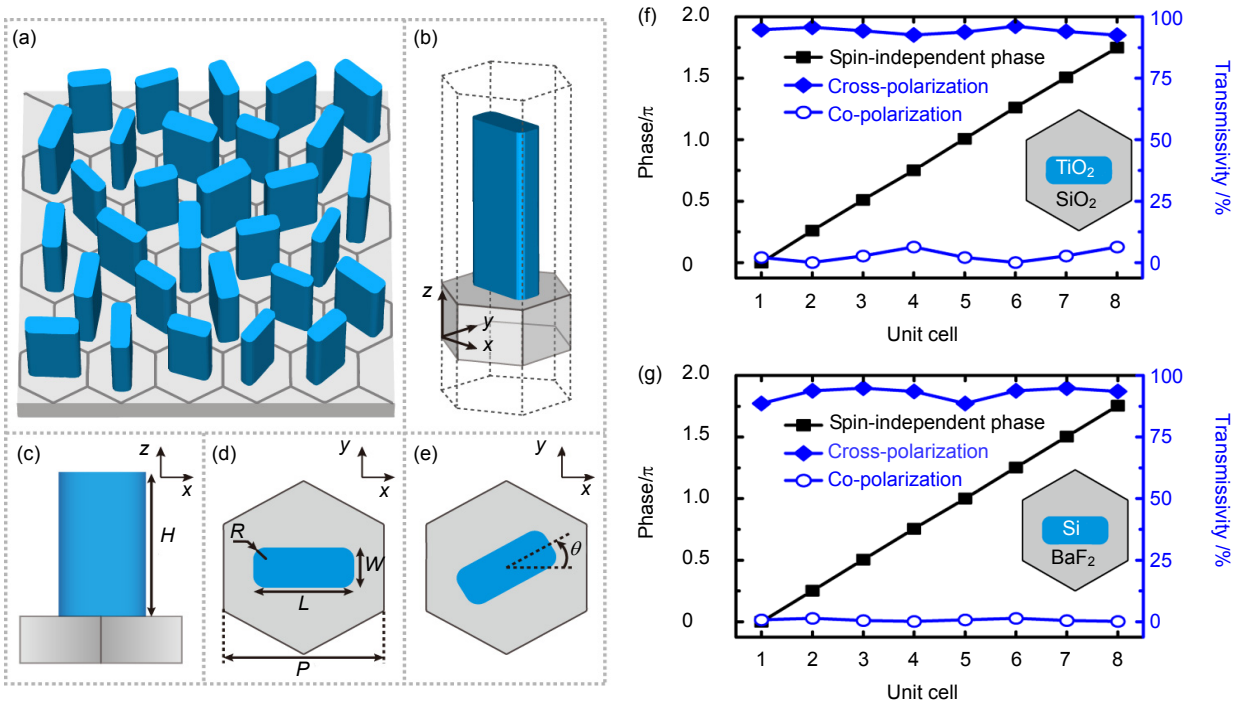

Fig. 1 Unit cell design. (a) Top view of the proposed metasurface consisting of chamfered nanofins on a substrate, with the same height and chamfering radius, but different sizes and orientations. (b) The nanofin is placed at the center of hexagonal unit cell. (c)~(e) Side and top views of hexagonal unit cell showing height H, width W, length L, chamfering radius R and rotation angle θ of the nanofin, with the lattice constant P. (f) The simulated spin-independent phases and cross-polarized and co-polarized transmissivities of eight unit cells at the wavelength of 532 nm. The materials of nanofins and substrate are titanium dioxide (TiO_2) and quartz (SiO_2), respectively. Constant parameters: H = 600 nm, P = 370 nm and R = 30 nm. The nanofins sizes (L and W) of unit cells from 1 to 4 are L = 300, 290, 235 and 240 nm, and W = 120, 105, 100 and 80 nm. (g) The simulated results of eight unit cells at the wavelength of 10.6 μm. The materials of nanofins and substrate are silicon (Si) and barium fluoride (BaF_2), respectively. Constant parameters: H = 7 μm, P = 4.8 μm, and R = 0.4 μm. The nanofins sizes (L and W) of unit cells from 1 to 4 are L = 3.8, 3.45, 3.15 and 3.6 μm, and W = 1.75, 1.6, 1.43 and 1 μm. The unit cells from 5 to 8 are acquired by rotating the posts from 1 to 4 by an angle of 90° clockwise in (f) and (g). Simulations use the finite element method (FEM) in CST microwave studio. The refractive indices are given as 2.43 (TiO_2), 1.46 (SiO_2), 3.42 (Si) and 1.40 (BaF_2), respectively.

vectorial angular spectrum theory [29] with the pixel of $(\sqrt{3}P/2)\times(\sqrt{3}P/2)$ (obtained by equivalent period of hexagonal arrangement in the free space), and the corresponding information for polarizations and phase shifts of unit cells are taken into account.

Chiral holograms based on geometric phase modulation have been reported in our previous works [18-19]. The different images for two opposite spins are obtained by special sections of the far field [17]. The holographic images generated by two circular polarizations are also central symmetric in fact, and each holographic image contains two desired images, leading to a decreased optical usage of incidence. Truly asymmetric holographic images for two opposite spins are shown in Fig. 2. Under the illumination of LCP incidence, the metasurfaces generate images of the badge of the Institute of Optics and Electronics, CAS at the far field, as shown in Figs. 2(a) and 2(c). In contrast, completely different images of the badge of the Chongqing University are obtained for another chirality, as illustrated in Figs. 2(b) and 2(d). The phase-only holograms of these two badges are acquired by the iterative Fourier-transform algorithm (IFTA) [30].

Multifocal lens has been widely used in imaging systems, detectors, and optical communications [31-35]. However, most of inhomogeneous and anisotropic metasurfaces [6-9], applied in focusing and imaging systems, are only suitable for one particular spin. For another, the transmitted light is scattered because of inverse symmetry phase gradients for two opposite spins created by traditional anisotropic structured metasurface. The dual-focal lens can be obtained by combining the two sets of patterns without overlapping with each other [33-35], with each corresponding to one focal point. However, it has a fatal flaw. The lens in a given region only contributes to corresponding focal point but adds background noise to another, resulting in a decreased optical usage of incidence. One dual-focal metalens that separates and focuses LCP and RCP portions at different points along transverse direction is presented in Fig. 3. Each nanofin can simultaneously contribute to two foci, leading to high efficiency and low noise. Furthermore, an array of foci can be obtained by using simulated annealing (SA) algorithm [36], Yang-Gu algorithm [37], or holography [38], in order to meet different needs for practical applications. The relationship between the phase distribution ψ_σ and coordinate x and y are written as

$$\psi_\sigma = (2\pi/\lambda)[\sqrt{(x-\sigma d)^2+(y-\sigma d)^2+f^2}-f], \quad (5)$$

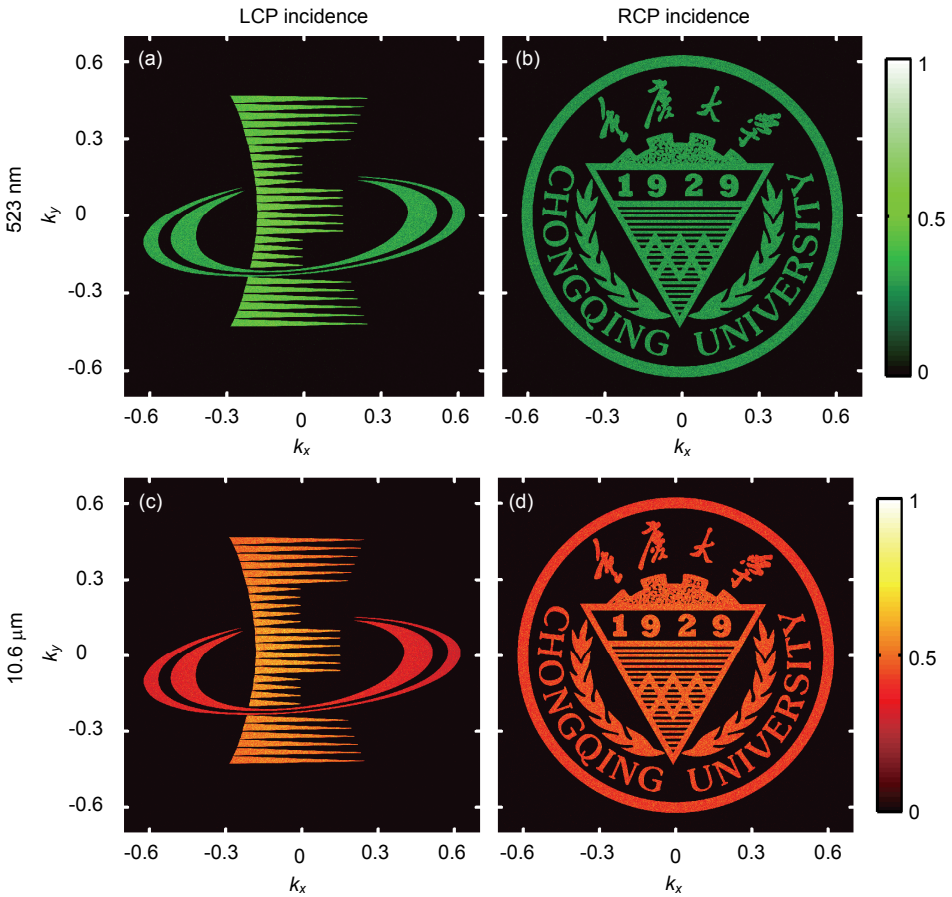

Fig. 2 Simulated results of holograms in the far field for circular polarizations at λ = 532 nm (2(a) and 2(b)) and λ = 10.6 μm (2(c) and 2(d)). The corresponding simulated sizes are 1 mm × 1 mm and 2 cm × 2 cm respectively for two working wavelengths (532 nm and 10.6 μm).

where f is focal length and d is lateral displacement of focal point.

Optical vortex has important applications in quantum optics, detection of rotating objects [39] and optical communication [40]. Our proposed method enables a new and distinctive feature, the generation of vortex beams carrying different and arbitrary OAMs for two opposite spins, which cannot be demonstrated by q-plates and traditional anisotropic structured metasurface. Fig. 4 shows that the proposed metasurfaces generate vortex beams with asymmetric topological charges for two opposite spins (l_{-1} = 6 for σ= −1 and l_1= −4 for σ= 1). In order to straightforwardly characterize the vortex beams, on-axis focusing phase gradient is superposed into total phase distribution and only the center zone (with the radius of just 0.5 times the radius of the device) carries OAM. In a word, the relationship between the phase distribution ψ_σ and coordinate x and y are given by

$$\psi_\sigma = \frac{2\pi}{\lambda}(\sqrt{x^2+y^2+f^2}-f)+ H(0.5R-\sqrt{x^2+y^2})l_\sigma\varphi \quad , \tag{6}$$

where R is the radius of metasurface, H is the step function; and φ is the azimuthal angle. On the basis of the interference effect, the topological charge of the OAM can be directly identified, without the use of additional interference beam [41]. The intensity patterns for different input beams were recorded at the focal plane nearby and in good agreement with the theoretical predictions. The intensity patterns are manifested by rotating petals encircling the beam centers, where the modulus and sign of l are determined by the number and twisting direction of these petals, respectively.

The dual-functional and/or multifunctional devices have huge fascinations and prospects to conveniently integrate and miniaturize complex systems with low costs. The asymmetric SOI allows not only dual-functional devices mentioned above but also other dual-functional or multifunctional shared-aperture devices without reduction of optical energy usage. For example, in our previous work [42], similar structures were used to achieve efficient generation and tight focusing of radially (or azimuthally) polarized beam from x- (or y-) polarized beam.

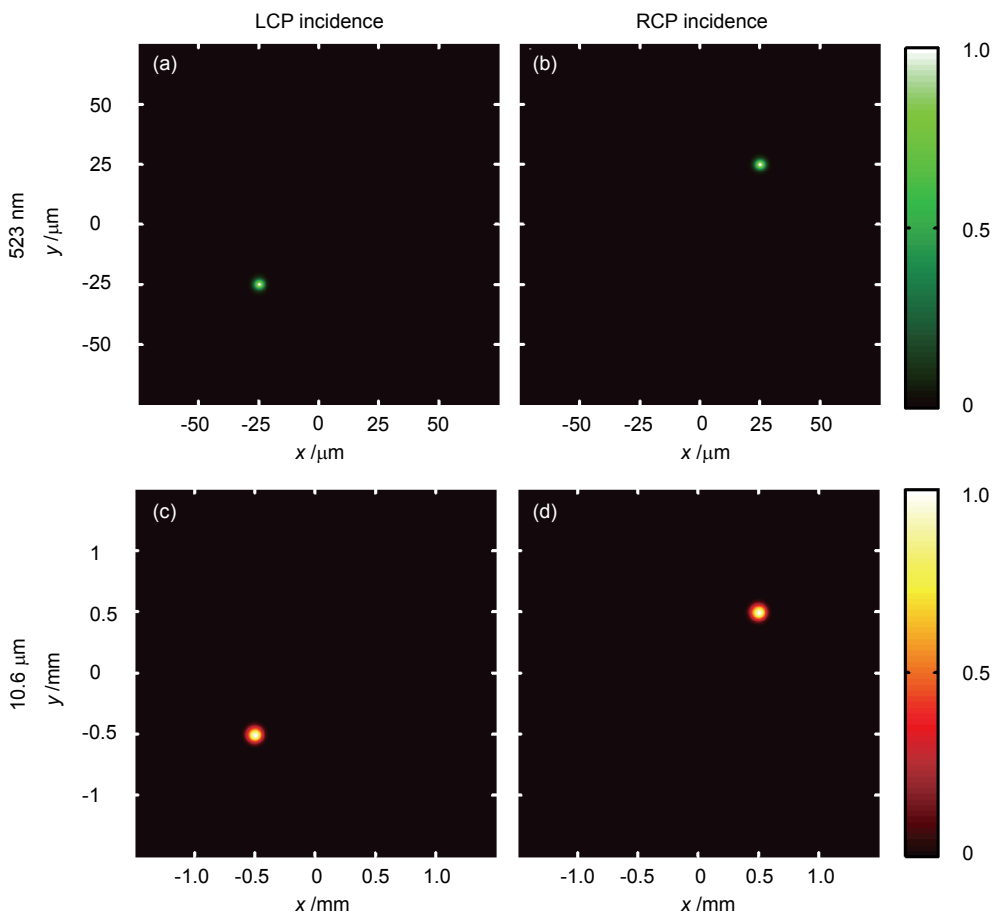

Fig. 3 Simulated intensity distributions in corresponding focal plane of dual-focal meta-lenses for circular polarizations at λ=532 nm (3(a) and 3(b)), and λ=10.6 μm (3(c) and 3(d)). The focal lengths of two meta-lenses are 5 mm and 10 cm, respectively. The simulated regions are circles whose diameters are 1 mm and 2 cm respectively for two working wavelengths (532 nm and 10.6 μm).

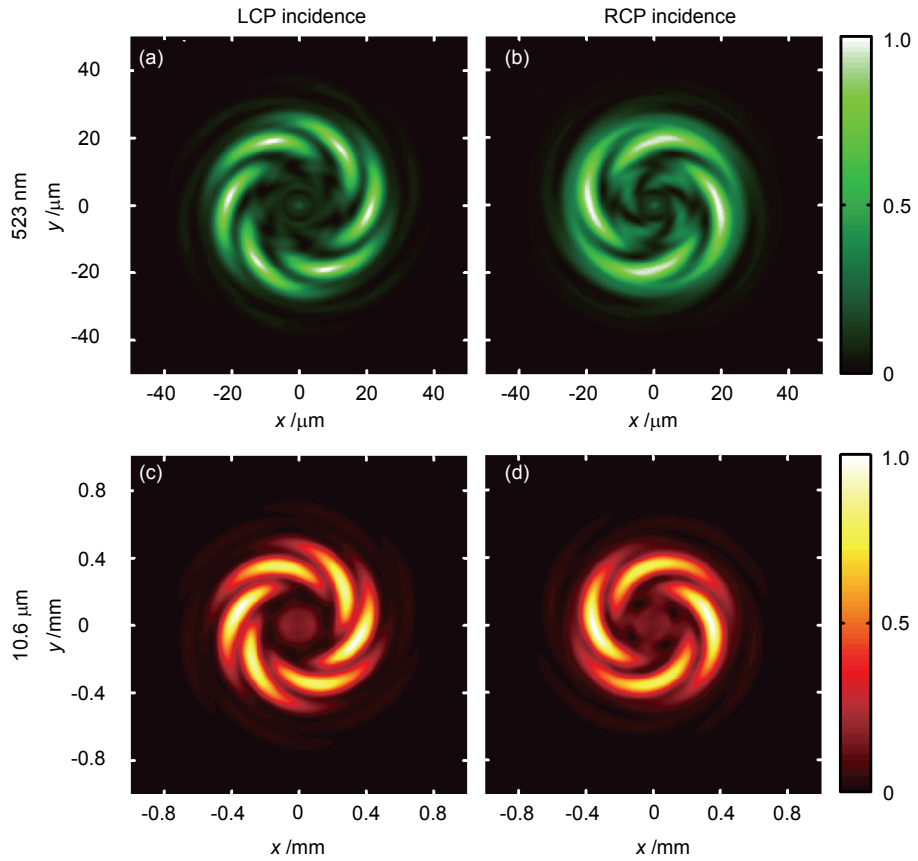

Fig. 4 Simulated results of optical vortex generation with asymmetric topological charges for circular polarizations at λ= 532 nm (4(a) and 4(b)), and λ= 10.6 μm (4(c) and 4(d)). The focal lengths of two meta-lenses are 5 mm and 10 cm, respectively. The simulated regions are circles whose diameters are 1 mm and 2 cm respectively for two working wavelengths (532 nm and 10.6 μm).

4 Conclusions

In summary, we present an all-dielectric metasurface platform, composed of an array of nanofins with spatially varying sizes and orientations, which can provide spin-independent phase gradient and spin-dependent geometric phase gradient, respectively. Owing to two phase gradients being independent, the final phase gradients for two opposite spins no longer have inverse symmetry and can be independently manipulated, resulting in asymmetric SOI of light for two opposite spins. Based on this specific design, we achieve three kinds of dual-functional devices with high efficiency at visible and infrared wavelengths: asymmetric holographic images, spin-selective focusing without the scattered noise, and generation of vortex beams with asymmetric topological charges. We believe that our design will find a large amount of applications in novel spin-controlled multi-functional shared-aperture devices, as well as open a new degree of freedom for the photonic applications of SOI. We noted that asymmetric holographic images using similar structures were reported during the revision process of our manuscript [43].

Acknowledgements

This work was supported by 973 Program of China (2013CBA01700) and National Natural Science Funds (61622508, 61575032).

References

1 Liberman V S, Zel'dovich B Y. Spin-orbit interaction of a photon in an inhomogeneous medium[J]. *Physical Review A*, 1992, **46**(8): 5199–5207.

2 Allen L, Barnett S M, Padgett M J. Optical angular momentum [M]. Boca Raton, FL: CRC Press, 2003.

3 Mair A, Vaziri A, Weihs G, *et al*. Entanglement of the orbital angular momentum states of photons[J]. *Nature*, 2001, **412**(6844): 313–316.

4 Pu Mingbo, Ma Xiaoliang, Li Xiong, *et al*. Merging plasmonics and metamaterials by two-dimensional subwavelength structures[J]. *Journal of Materials Chemistry C*, 2017: 10.1039/C7TC00440K.

5 Luo Xiangang. Principles of electromagnetic waves in metasurfaces[J]. *Science China Physics, Mechanics & Astronomy*, 2015, **58**(9): 594201.

6 Luo Jun, Zeng Bo, Wang Changtao, *et al*. Fabrication of anisotropically arrayed nano-slots metasurfaces using reflective

plasmonic lithography[J]. *Nanoscale*, 2015, **7**(44): 18805–18812.

7 Tang Dongliang, Wang Changtao, Zhao Zeyu, *et al*. Ultrabroadband superoscillatory lens composed by plasmonic metasurfaces for subdiffraction light focusing[J]. *Laser & Photonics Reviews*, 2015, **9**(6): 713–719.

8 Zhao Zeyu, Pu Mingbo, Gao Hui, *et al*. Multispectral optical metasurfaces enabled by achromatic phase transition[J]. *Scientific Reports*, 2015, **5**: 15781.

9 Khorasaninejad M, Chen Weiting, Devlin R C, *et al*. Metalenses at visible wavelengths: diffraction-limited focusing and subwavelength resolution imaging[J]. *Science*, 2016, **352**(6290): 1190–1194.

10 Ma Xiaoliang, Pu Mingbo, Li Xiong, *et al*. A planar chiral meta-surface for optical vortex generation and focusing[J]. *Scientific Reports*, 2014, **5**: 10365.

11 Pu Mingbo, Li Xiong, Ma Xiaoliang, *et al*. Catenary optics for achromatic generation of perfect optical angular momentum[J]. *Science Advances*, 2015, **1**(9): e1500396.

12 Guo Yinghui, Yan Lianshan, Pan Wei, *et al*. Generation and manipulation of orbital angular momentum by all-dielectric metasurfaces[J]. *Plasmonics*, 2016, **11**(1): 337–344.

13 Jin Jinjin, Pu Mingbo, Wang Yanqin, *et al*. Multi-channel vortex beam generation by simultaneous amplitude and phase modulation with two-dimensional metamaterial[J]. *Advanced Materials Technologies*, 2017, **2**(2): 1600201.

14 Guo Yinghui, Pu Mingbo, Zhao Zeyu, *et al*. Merging geometric phase and plasmon retardation phase in continuously shaped metasurfaces for arbitrary orbital angular momentum generation [J]. *ACS Photonics*, 2016, **3**(11): 2022–2029.

15 Pu Mingbo, Chen Po, Wang Yanqin, *et al*. Anisotropic meta-mirror for achromatic electromagnetic polarization manipulation[J]. *Applied Physics Letters*, 2013, **102**(13): 131906.

16 Guo Yinghui, Wang Yanqin, Pu Mingbo, *et al*. Dispersion management of anisotropic metamirror for super-octave bandwidth polarization conversion[J]. *Scientific Reports*, 2014, **5**: 8434.

17 Wen Dandan, Yue Fuyong, Li Guixin, *et al*. Helicity multiplexed broadband metasurface holograms[J]. *Nature Communications*, 2015, **6**: 8241.

18 Zhang Xiaohu, Jin Jinjin, Pu Mingbo, *et al*. Ultrahigh-capacity dynamic holographic displays via anisotropic nanoholes[J]. *Nanoscale*, 2017, **9**(4): 1409–1415.

19 Li Xiong, Chen Lianwei, Li Yang, *et al*. Multicolor 3D meta-holography by broadband plasmonic modulation[J]. *Science Advances*, 2016, **2**(11): e1601102.

20 Pu Mingbo, Zhao Zeyu, Wang Yanqin, *et al*. Spatially and spectrally engineered spin-orbit interaction for achromatic virtual shaping[J]. *Scientific Reports*, 2014, **5**: 9822.

21 Guo Yinghui, Yan Lianshan, Pan Wei, *et al*. Scattering engineering in continuously shaped metasurface: an approach for electromagnetic illusion[J]. *Scientific Reports*, 2016, **6**: 30154.

22 Pancharatnam S. Generalized theory of interference, and its applications. Part I. Coherent pencils[J]. *Proceedings of the Indian Academy of Sciences-Section A*, 1956, **44**(5): 247–262.

23 Berry M V. Quantal phase factors accompanying adiabatic changes[J]. *Proceedings of the Royal Society A: Mathematical, Physical and Engineering Sciences*, 1984, **392**(1802): 45–57.

24 Kang Ming, Feng Tianhua, Wang Huitian, *et al*. Wave front engineering from an array of thin aperture antennas[J]. *Optics Express*, 2012, **20**(14): 15882–15890.

25 Khorasaninejad M, Crozier K B. Silicon nanofin grating as a miniature chirality-distinguishing beam-splitter[J]. *Nature Communications*, 2014, **5**: 5386.

26 Lin Dianmin, Fan Pengyu, Hasman E, *et al*. Dielectric gradient metasurface optical elements[J]. *Science*, 2014, **345**(6194): 298–302.

27 Luo Xiangang, Pu Mingbo, Li Xiong, *et al*. Broadband spin Hall effect of light in single nanoapertures[J]. *Light: Science & Applications*, 2017, **6**: e16276.

28 Arbabi A, Horie Y, Bagheri M, *et al*. Dielectric metasurfaces for complete control of phase and polarization with subwavelength spatial resolution and high transmission[J]. *Nature Nanotechnology*, 2015, **10**(11): 937–943.

29 Ciattoni A, Crosignani B, Di Porto P. Vectorial free-space optical propagation: a simple approach for generating all-order nonparaxial corrections[J]. *Optics Communications*, 2000, **177**(1–6): 9–13.

30 Gerchberg R W, Saxton W O. A practical algorithm for the determination of phase from image and diffraction plane pictures[J]. *Optik*, 1972, **35**(2): 237–246.

31 Valle P J, Cagigal M P. Analytic design of multiple-axis, multifocal diffractive lenses[J]. *Optics Letters*, 2012, **37**(6): 1121–1123.

32 de Gracia P, Dorronsoro C, Marcos S. Multiple zone multifocal phase designs[J]. *Optics Letters*, 2013, **38**(18): 3526–3529.

33 Chen Xianzhong, Chen Ming, Mehmood M Q, *et al*. Longitudinal multifoci metalens for circularly polarized light[J]. *Advanced Optical Materials*, 2015, **3**(9): 1201–1206.

34 Wang Wei, Guo Zhongyi, Zhou Keya, *et al*. Polarization-independent longitudinal multi-focusing metalens[J]. *Optics Express*, 2015, **23**(23): 29855–29866.

35 Khorasaninejad M, Chen W T, Zhu A Y, *et al*. Multispectral chiral imaging with a metalens[J]. *Nano Letters*, 2016, **16**(7): 4595–4600.

36 Zhu Qiaofen, Wang Dayong, Zheng Xianhua, *et al*. Optical lens design based on metallic nanoslits with variant widths[J]. *Applied Optics*, 2011, **50**(13): 1879–1883.

37 Zhu Qiaofen, Ye Jiasheng, Wang Dayong, *et al*. Optimal design of SPP-based metallic nanoaperture optical elements by using Yang-Gu algorithm[J]. *Optics Express*, 2011, **19**(10): 9512–9522.

38 Pang Hui, Gao Hongtao, Deng Qiling, *et al*. Multi-focus plasmonic lens design based on holography[J]. *Optics Express*, 2013, **21**(16): 18689–18696.

39 Lavery M P J, Speirits F C, Barnett S M, *et al*. Detection of a spinning object using light's orbital angular momentum[J]. *Science*, 2013, **341**(6145): 537–540.

40 Bozinovic N, Yue Yang, Ren Yongxiong, *et al*. Terabit-scale orbital angular momentum mode division multiplexing in fibers[J]. *Science*, 2013, **340**(6140): 1545–1548.

41 Franke-Arnold S, Allen L, Padgett M. Advances in optical angular momentum[J]. *Laser & Photonics Reviews*, 2008, **2**(4): 299–313.

42 Zhang Fei, Yu Honglin, Fang Jiawen, *et al*. Efficient generation and tight focusing of radially polarized beam from linearly polarized beam with all-dielectric metasurface[J]. *Optics Express*, 2016, **24**(6): 6656–6664.

43 Mueller J P B, Rubin N A, Devlin R C, *et al*. Metasurface polarization optics: independent phase control of arbitrary orthogonal states of polarization[J]. *Physical Review Letters*, 2017, **118**(11): 113901.